JACC: CARDIOVASCULAR IMAGING
VOL. 9, NO. 7, 2016

ISSN 1936-878X/$36.00
PUBLISHED BY ELSEVIER
http://dx.doi.org/10.1016/j.jcmg.2015.12.018

Myocardial Characterization Using Dual-Energy CT in Doxorubicin-Induced DCM

Comparison With CMR T1-Mapping and Histology in a Rabbit Model

Yoo Jin Hong, MD, PhD,[a] Tai Kyung Kim, DVM,[b] Donghyun Hong, MS,[c] Chul Hwan Park, MD,[d] Sae Jong Yoo, DVM,[b] Mary Ellen Wickum, MS,[a] Jin Hur, MD, PhD,[a] Hye-Jeong Lee, MD, PhD,[a] Young Jin Kim, MD, PhD,[a] Young Joo Suh, MD,[a] Andreas Greiser, PhD,[e] Mun Young Paek, MS,[f] Byoung Wook Choi, MD, PhD[a]

ABSTRACT

OBJECTIVES This study sought to evaluate whether patterns of myocardial change in doxorubicin-induced dilated cardiomyopathy determined using dual-energy computed tomography (CT) were similar to characterization by extracellular volume fraction (ECV) using cardiac magnetic resonance (CMR) T1-mapping and collagen volume fraction (CVF) measured using histology.

BACKGROUND Anthracycline chemoagents are effective against a wide range of malignant conditions. However, cardiotoxicity is a well-known adverse effect of these drugs. Dual-energy CT could be as useful as magnetic resonance (MR) to evaluate myocardial change in anthracycline-induced cardiotoxicity.

METHODS A dilated cardiomyopathy rabbit model was generated by injecting 11 adult New Zealand rabbits with 1.0 mg/kg of doxorubicin twice weekly for 16 weeks. Contrast-enhanced dual-energy CT and pre-contrast and post-contrast T1-mapping CMR using a prototype modified Look-Locker inversion recovery on a clinical 3-T scanner were performed on 15 rabbits, including 4 control animals, to calculate ECV at baseline, and at 6, 12, and 16 weeks after doxorubicin administration.

RESULTS The mean ECV values (%) on CT and CMR at 6, 12, and 16 weeks after modeling were significantly higher than those measured at baseline (CT ECV: 35.3%, 41.9%, 42.1% vs. 28.5%; MR ECV: 32.6%, 35.8%, 41.3% vs. 28.8%, respectively; all $p < 0.001$). CT ECV and MR ECV values were well correlated ($r = 0.888$; $p < 0.001$). Both were well correlated with CVF on histology (CT ECV vs. CVF, $r = 0.925$, $p < 0.001$ and MR ECV vs. CVF, $r = 0.961$, $p < 0.001$, respectively).

CONCLUSIONS Dual-energy CT ECV correlated well with CMR and histology. Dual-energy CT is useful for characterizing doxorubicin-induced cardiomyopathy by measuring ECV fraction; however, further technical improvements are desirable to lower motion artifact and improve image quality of the iodine map. (J Am Coll Cardiol Img 2016;9:836–45)

From the [a]Department of Radiology and Research Institute of Radiological Science, Severance Hospital, Yonsei University College of Medicine, Seoul, South Korea; [b]Department of Veterinary Surgery, College of Veterinary Medicine, Konkuk University, Seoul, Korea; [c]Erwin L. Hahn Institute for Magnetic Resonance Imaging, University of Duisburg-Essen, Essen, Germany; [d]Department of Radiology and Research Institute of Radiological Science, Gangnam Severance Hospital, Yonsei University College of Medicine, Seoul, South Korea; [e]Siemens AG Healthcare, Erlangen, Germany; and [f]Siemens Ltd., Seoul, Korea. This study was supported by the Research Institute of Radiological Science, Yonsei University College of Medicine, and a grant from Dong-kook Pharmaceutical, Seoul, South Korea. All authors have reported that they have no relationships relevant to the contents of this paper to disclose.

Manuscript received May 8, 2015; revised manuscript received November 30, 2015, accepted December 11, 2015.

Anthracycline chemoagents are effective against a wide range of malignant conditions (1). However, cardiotoxicity is a well-known adverse effect of these drugs that causes diffuse and irreversible myocardial fibrosis (2). This damage to the myocardial structure is known to be associated with adverse cardiac events (3,4).

Myocardial T1-mapping cardiac magnetic resonance (CMR) is an emerging technique that could improve detection of diffuse interstitial myocardial fibrosis caused by chemotherapy-induced cardiotoxicity by measuring the extracellular volume (ECV) fraction (5,6). A few recent studies used computed tomography (CT) to detect diffuse myocardial fibrosis (7,8). These studies were based on the theory that iodine contrast agents used in CT and gadolinium agents used in CMR, despite their different molecular structures (9), have similar kinetics, molecular weights, and ECV of distribution.

SEE PAGE 846

Dual-energy CT is an advanced imaging technique that can provide additional information regarding material composition using 2 different x-ray spectra data sets (10). There are no prior reports on the quantification of the ECV using dual-energy CT in diffuse myocardial fibrosis patients.

We hypothesized that dual-energy CT would be valuable for extracting the iodine component of the myocardium, and for assessing CT ECV in a doxorubicin-induced cardiomyopathy model. Accordingly, this study aimed to validate ECV using dual-energy CT, to compare CT ECV with parallel contrast-enhanced CMR measurements, and to assess histological collagen volume fraction (CVF) in a rabbit model of doxorubicin-induced dilated cardiomyopathy (DCM).

METHODS

ANIMAL MODELING AND EXPERIMENT FLOW CHART. All experiments were approved by the animal care and use committee at our institution and experiments were performed according to the National Institutes of Health guidelines. Twenty adult male New Zealand white rabbits weighing 3 to 4 kg were included. Among them, 4 rabbits served as control subjects for histological evaluations. The remaining 16 rabbits received 1.0 mg/kg injections of doxorubicin (doxorubicin hydrochloride, Cayman Chemical, Ann Arbor, Michigan) twice weekly until they were sacrificed for histological evaluations (11). For drug administration, the auricular vein was accessed by introduction of a 21-gauge needle. Doxorubicin (1.0 mg/kg) was diluted in 20 ml of 0.9% sterile saline and slowly injected over 3 min using the bolus injection method.

Among the 16 rabbits, 5 died during the modeling period from severe anemia (n = 3) or infection (pneumonia, n = 2). At the end of the 6-week modeling period, the remaining subjects (n = 11) underwent post-modeling CT and CMR scans. Subsequently, 3 rabbits were sacrificed for histological evaluation. The remaining rabbits (n = 8) continued DCM modeling, and underwent scans at the end of the 12-week modeling period. An additional 3 rabbits were sacrificed at 12 weeks. The remaining rabbits continued DCM modeling (n = 5), and underwent scans at the end of the 16-week modeling period. Afterward the 5 remaining rabbits were sacrificed for histological evaluation (Figure 1).

CT AND MR IMAGING EXAMINATIONS. The rabbits underwent CT and magnetic resonance (MR) examination before drug administration (control subject), and at the end of specific

ABBREVIATIONS AND ACRONYMS

CMR = cardiac magnetic resonance
CT = computed tomography
CVF = collagen volume fraction
DCM = dilated cardiomyopathy
ECV = extracellular volume fraction
Hct = hematocrit
HU = Hounsfield unit
ICC = intraclass correlation coefficient
LGE = late gadolinium enhancement
LV = left ventricle
LVEF = left ventricular ejection fraction
MR = magnetic resonance
ROI = regions of interest

FIGURE 1 Experiment Flow Chart

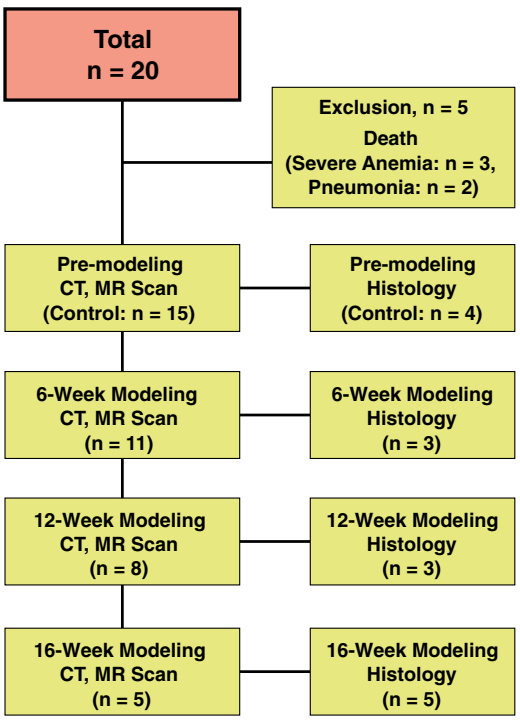

The process of the experiment of the CT, MR scanning, and histological examination in rabbit models. CT = computed tomography; MR = magnetic resonance.

post-modeling intervals (6, 12, or 16 weeks after DCM modeling). Before CT examination, the rabbits were anesthetized with an intramuscular injection of tiletamine, 30 mg/kg (Zoletil, Vibac Laboratories, Carros, France) and xylazine, 5 mg/kg (Rompun, Bayer, Seoul, Korea), and the anterior chest wall of each rabbit was shaved for electrocardiogram electrodes placement. Both auricular veins of each rabbit were prepared for venous access for contrast injection and administration of medetomidine hydrochloride, 0.3 mg/kg (Tomidine, Provet Veterinary Products Ltd., Istanbul, Turkey). Venous sampling was performed to obtain hematocrit (Hct) values for all rabbits immediately before the CT examinations. The animals were intubated and mechanically ventilated (Mekant, MEKICS, Seoul, Korea) using a mixture of oxygen and isoflurane. The ventilator was not CMR-compatible and was thus placed outside the CMR room with the long respiratory tubes entering the room.

CT PROTOCOL. Dual-energy CT was performed using a dual-source CT (Somatom Definition Flash, Siemens Healthcare, Forchheim, Germany) with retrospective electrocardiogram-gated scanning. Scan parameters were as follows: 185 effective mA at 100 kV, and 157 effective mA at 140 kV with a tin filter, 64 × 0.6 mm collimation, 0.32 pitch factor, and 0.28-s rotation time. After a bolus injection of 2 ml/kg contrast medium (Pamiray 370, Dongkook Pharmaceutical, Seoul, Korea), 8 to 10 ml of normal saline was infused at a rate of 1.5 to 1.7 ml/s through the auricular vein of each rabbit. The initial post-contrast scan started at 3 min, and additional scans were obtained at 5, 7, 9, 11, 13, and 20 min after contrast injection. Each rabbit was administered a bolus injection of 0.3 mg/kg of medetomidine to reduce heart rate 30 s before each scan.

Dual-energy CT data post-processing. All CT data were processed on a dedicated workstation equipped with dual-energy post-processing software (syngo MMWP VE 36A, Siemens Healthcare). The Online Appendix provides detailed steps.

CMR PROTOCOL. CMR was performed immediately after dual-energy CT and completed within 2 h. A 3.0-T MR scanner (Magnetom Trio Tim, Siemens Healthcare, Erlangen, Germany) with a 6-channel anterior body matrix coil, and the posterior part of a 12-channel head matrix coil was used. Localization of the heart was achieved using a steady-state free precession sequence under electrocardiogram gating. Cine, late gadolinium enhancement (LGE), and pre-contrast and post-contrast T1-mapping images were acquired. For cardiac functional analysis, cine images were acquired using a TrueFISP sequence in the short-axis plane orientation. T1-mapping was performed using a prototype modified Look-Locker inversion recovery sequence during the end-expiratory period in short axis view at mid-ventricle. Pre-contrast T1-mapping images were acquired before the injection of contrast. Post-contrast T1-mapping images were acquired 1, 3, 5, 7, 9, 11, 13, and 20 min after the injection of a 0.2 mmol/kg intravenous dose of gadolinium contrast agent (Omniscan, GE Healthcare, Princeton, New Jersey). LGE imaging was obtained 15 min after the injection of the contrast agent using a magnitude- and phase-sensitive inversion recovery-prepared steady-state free precession sequence (see the Online Appendix for the detail protocol).

IMAGE ANALYSIS. Two radiologists (Y.J.H., C.H.P.), both of whom had 9 years of experience in cardiovascular image interpretation, analyzed all images.

CT image analysis. CT ECV (%) and post-contrast Hounsfield unit (HU) were measured on a PACS system. The same image, with MR short axis mid-left ventricle (LV) where the papillary muscles were visible, was chosen from the 13-min iodine map and post-contrast image. The regions of interest (ROI) were drawn at the septal segment, and a round ROI (≥10 mm^2) that avoided the papillary muscle was drawn in the LV cavity (**Figure 2A**). The mean attenuation at the ROI was recorded in HU. Myocardial CT ECV (ECV_m) was calculated using the following formula (Equation 1):

$$ECV_m = (HU_m/HU_b) \times (1 - Hct)$$

where ECV_m is myocardial ECV in dual-energy CT, HU_m is HU corresponding to the myocardium ROI on the iodine map, and HU_b is HU corresponding to the blood pool on the iodine map.

CT ECV map software development. CT ECV maps were quantified by a custom-developed software package written in MATLAB version 2014a (The MathWorks, Inc., Natick, Massachusetts). The Online Appendix provides detailed steps.

Evaluation of the image quality of the CT iodine map and T1 map images. The image quality of the iodine maps generated 3, 5, 7, 9, 11, 13 and 20 min after contrast injection was determined using a subjective 4-point scale based on image degradation and demarcation between the LV myocardium and cavity. According to the scale, 4 = excellent, no image degradation, clear demarcation between LV myocardium and cavity; 3 = good, minor degree of image degradation without affecting diagnostic accuracy; 2 = adequate, moderate degree of image degradation that slightly affected

FIGURE 2 Measurement on CT and Cardiac Magnetic Resonance

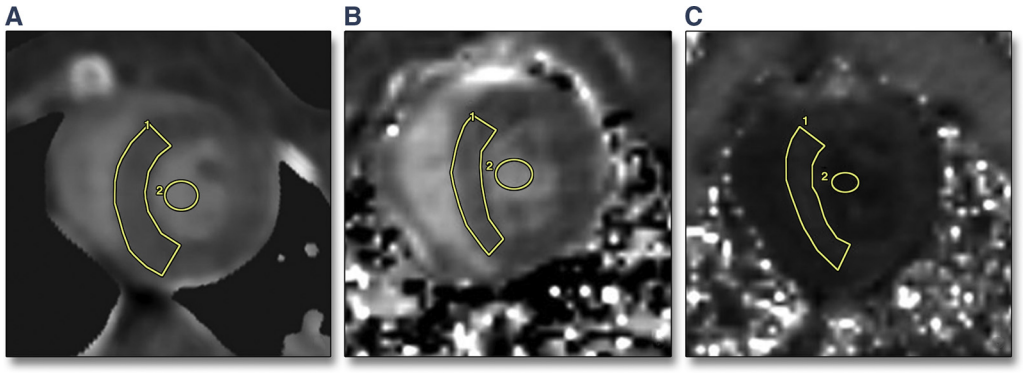

(A) The CT regions of interest were drawn at the septal segment and cavity of left ventricle on the iodine map. On the pre-contrast T1-map **(B)** and post-contrast T1-map CMR images **(C)**, regions of interest were drawn at the same areas as the CT. Abbreviations as in Figure 1.

diagnostic accuracy but images were still used for diagnosis; and 1 = poor, severe image degradation that greatly affected diagnostic accuracy and resulted in nondiagnostic poor images. Pre-T1 and post-T1 map CMR images were scored using the Peter Kellman scale (12). Online Figure 1 shows representative images of iodine maps and the image qualities of CMR map images.

Functional CMR image analysis. All CMR cine images were transferred to commercially available software (Argus, Siemens Medical Solutions, Erlangen, Germany). The LV function was assessed on the short-axis cine CMR images using the Simpson method.

CMR image analysis for the measurement of ECV fraction (%). All CMR images were transferred to a PACS system for image analysis. The ROIs at the same septal segment measured on CT were drawn on the pre-contrast and post-contrast T1-mapping image at the mid-LV where papillary muscles were visible. For a measurement of the T1 blood value, a round ROI (≥5 mm^2) that avoided papillary muscles was drawn in the LV cavity (Figures 2B and 2C). The ECV fraction was calculated from Equation 2 as follows:

$$\mathrm{ECV} = \left[\left(1/\mathrm{T1}_{\text{post-contrastmyocardium}}\right) - \left(1/\mathrm{T1}_{\text{pre-contrastmyocardium}}\right)\right] / \left[\left(1/\mathrm{T1}_{\text{post-contrastblood}}\right) - \left(1/\mathrm{T1}_{\text{pre-contrastblood}}\right)\right] \times (1-\mathrm{Hct})$$

HISTOLOGICAL ANALYSIS. For histology, samples from the LV were obtained immediately after euthanasia accomplished by KCl injection, and fixed in 10% phosphate buffered paraformaldehyde. After 1 week of fixation, the tissue was dissected at the short axis plane at mid-LV level where the papillary muscles were visible, using a rabbit heart slicer (Zivic Instruments, Pittsburgh, Pennsylvania). The fragments were dehydrated in solutions of decreasing alcohol concentration, cleared in xylene, and embedded in paraffin. Ten-micrometer sections were obtained and prepared for analysis by picrosirius red staining.

CVF (%) analysis. An independent researcher blinded to the CT and CMR results performed the histological analyses. Each histological section was obtained at the septal segment at mid-LV. Histopathologic image analyses were performed using ImageJ (National Institutes of Health, Bethesda, Maryland). The Online Appendix provides detailed steps.

STATISTICAL ANALYSES. All continuous data were expressed as the mean ± SD, and categorical variables were presented as numbers or percentages. CT ECV and MR ECV at 13 min were compared with histologic CVF using Spearman correlation. The correlation between myocardial CT ECV and MR ECV at 13 min was also assessed using a mixed model by the Hamlett method to account for repeated measurements over several weeks (13). The change in CT ECV values according to the scan time and the change in CT ECV, post-contrast HU, MR ECV, and pre-T1 values according to the modeling time (between control and 6, 12, and 16 weeks after modeling) were evaluated by a linear mixed model with restricted maximum likelihood estimation using the MIXED procedure in SAS version 9.2 (SAS Institute, Cary, North Carolina). The linear mixed model included fixed effects for time, and random intercept for each animal. Time was considered as a categorical variable in the model and the covariance was assumed to be equal among all time points.

Agreement between the measures of CT, MR ECV, pre-T1, and post-contrast HU between the 2 observers was assessed using the intraclass correlation coefficient (ICC) and Bland-Altman plot (14). The receiver operating characteristic curve was reconstructed using the Obuchowski method to compare the diagnostic performance of CT ECV and MR ECV with that of the left ventricular ejection fraction (LVEF) for the diagnosis of modeling subjects (15). All statistical analyses were performed using Statistical Package for the Social Science software version 20 (SPSS Inc., Chicago, Illinois) and SAS version 9.2 (SAS Institute Inc.), and $p < 0.05$ was considered statistically significant.

RESULTS

PHYSIOLOGICAL AND FUNCTIONAL DATA. The Hct levels in DCM rabbits were lower than those in control subjects. The Hct level of control subjects was 42.3% (36.9% to 54.8%), whereas that of 6-week model was 33.2% (18.7% to 46.2%) (Table 1). In the DCM rabbit model, ventricular chamber enlargement and LV wall thinning were noted. The mean LVEF for post-modeling subjects was significantly lower than the control subjects (Table 1).

DUAL-ENERGY CT VERSUS CMR. Validation of CT and CMR protocol. The CT ECV results revealed no significant changes from 3 min to 20 min in all subjects (control subject, $p = 0.208$; 6-week modeling subjects, $p = 0.827$; 12-week modeling subjects, $p = 0.877$; 16-week modeling subjects, $p = 0.916$). MR ECV results also revealed no significant changes from 3 min to 20 min in all subjects (control subject, $p = 0.782$; 6-week modeling subjects, $p = 0.894$; 12-week modeling subjects, $p = 0.691$; 16-week modeling subjects, $p = 0.831$) (Figures 3A to 3D).

Image quality of CT iodine maps. In total, 254 septal segments on the iodine map were analyzed across all subjects. Of these, 238 segments (93.7%) were of diagnostic quality (score = 2 to 4). Specifically, 61 segments (24.0%) were excellent (score = 4), 106 segments (41.7%) were good (score = 3), 71 segments (28.0%) were adequate (score = 2), and 16 segments (6.3%) were nondiagnostic (score = 1). Nondiagnostic segments were excluded from the image analysis.

Dual-energy CT and MR: ECV comparison. The mean CT ECV of the control subjects (n = 15) was 28.5% (25.9% to 31.3%) and that of 6-, 12-, and 16-week models was 35.3% (30.2% to 40.1%), 41.9% (35.6% to 44.1%), and 42.1% (39.2% to 46.4%), respectively. The mean MR ECV of the control subjects (n = 15) was 28.8% (26.1% to 30.8%) and that of 6-, 12-, and 16-week models was 32.6% (29.9% to 34.3%), 35.8% (31.0% to 39.8%), and 41.3% (38.4% to 47.3%), respectively (Table 2). Figure 4 shows the serial change in color maps of the LV according to the modeling time and ECV values. The interobserver agreement for CT and MR ECV measurements was good (ICC 0.902 [95% confidence interval (CI): 0.920 to 0.947] for CT ECV; ICC 0.953 (95% CI: 0.911 to 0.975) for MR ECV). A good correlation existed between CT ECV and MR ECV across all subjects (n = 26; $r = 0.888$; $p < 0.001$), and across post-modeling subjects (n = 11; $r = 0.840$; $p < 0.001$). Bland-Altman plots between CT and MR ECV showed small bias (1.406%) with 95% limits of agreement from -3.457% to 6.269% between CT and MR ECV (Figure 5).

Dual-energy CT and MR: other values and diagnostic performance. The mean post-contrast HU of control subjects was 58.0 HU (range 51 to 70 HU) and that of 6-, 12-, and 16-week models was 60.2 HU (range 50 to 77 HU), 68.4 (range 61.2 to 76.9 HU), and 69.4 (range 62.6 to 73.1 HU), respectively. The mean pre-T1 value of control subjects was 1,068.1 ms (range 1,030.0 to 1,103.85 ms) and that of 6-, 12-, and 16-week models was 1,110.3 ms (range 1,075.2 to 1,175.0 ms), 1,118.2 ms (range 1,059.2 to 1,160.8 ms), and 1,121.3 ms (range 1,104.5 to 1,121.8 ms), respectively. The ICC for pre-T1 value was 0.628 (95% CI: 0.393 to 0.786) and that for post-contrast HU was 0.727 (95% CI: 0.536 to 0.847).

The mean post-contrast HU of 12- and 16-week models was significantly higher than that of the control subjects, and the mean pre-T1 value of all post-modeling subjects was significantly higher than that of the control subject (Table 2). In LGE imaging, there was no focal LGE in the post-models. When we used CT ECV, MR ECV, and LVEF for diagnosis of post-modeling subjects, the areas under the receiver operating characteristic curve of CT ECV, MR ECV, and LVEF were 0.997 (95% CI: 0.990 to 1.000), 1.000 (95% CI: 1.000 to 1.000), and

TABLE 1 Physiological and Functional Data For All Subjects

	Control Subjects (n = 15)	6-Week Model (n = 11)	12-Week Model (n = 8)	16-Week Model (n = 5)
Hematocrit, %	42.3 (36.9-54.8)	33.2 (18.7-46.2)	33.0 (24.9-42.1)	37.3 (25.4-43.0)
Left ventricular ejection fraction, %	54.7 ± 3.2	44.3 ± 4.3*	36.2 ± 9.3†	32.0 ± 11.0‡
End-diastolic volume, ml	2.3 ± 0.8	2.0 ± 0.7	2.3 ± 0.6	3.1 ± 0.9
End-systolic volume, ml	1.0 ± 0.4	1.2 ± 0.4	1.6 ± 0.8	2.0 ± 0.6
Stroke volume, ml	1.2 ± 0.4	0.9 ± 0.3	0.7 ± 0.2	1.1 ± 0.3
Cardiac output, ml/min	273.7 ± 85.7	168.2 ± 57.0	120.9 ± 39.5	148.4 ± 34.1
Left ventricle mass, g/kg	0.8 ± 0.1	0.9 ± 0.2	1.1 ± 0.2	1.1 ± 0.2

Values are median (range) or mean ± SD. *Control vs. 6-week model, $p < 0.05$. †Control vs. 12-week model, $p < 0.05$. ‡Control vs. 16-week model, $p < 0.05$.

FIGURE 3 Change in CT, MR ECV Over Time After Contrast Injection

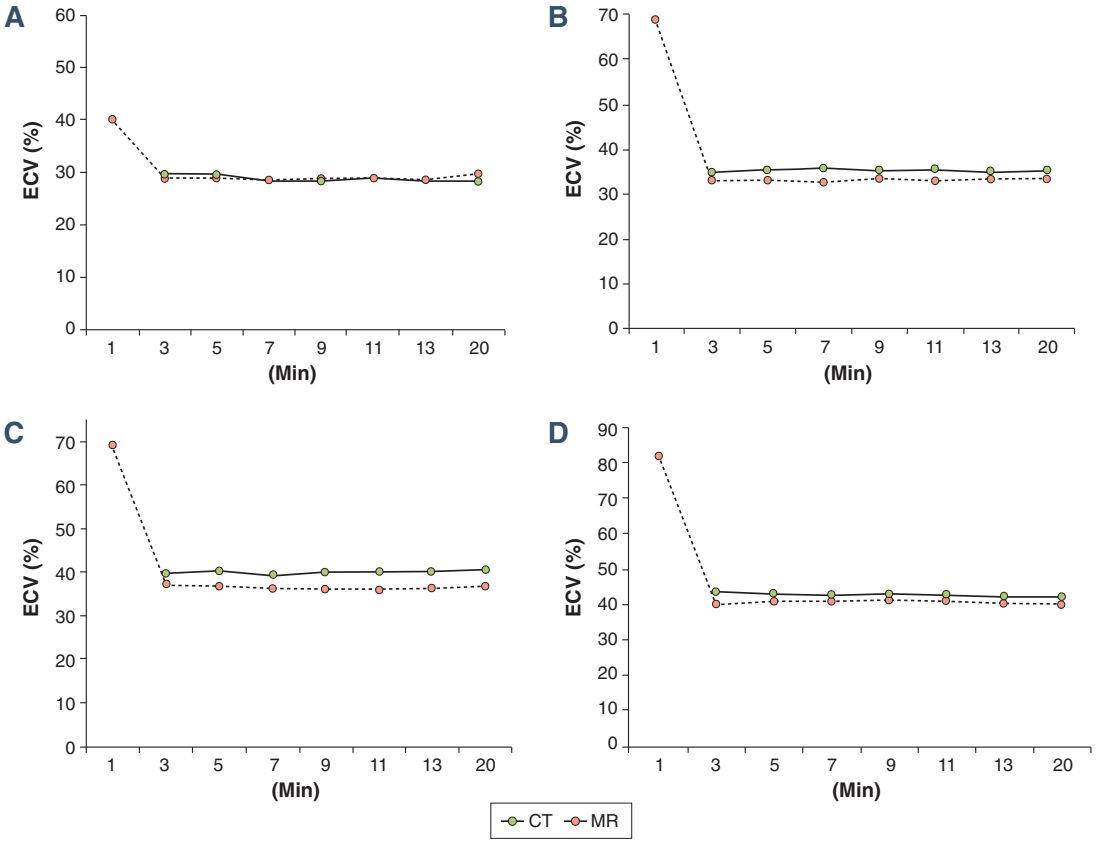

Mean CT and MR ECV did not change significantly at 3 to 20 min in control and models. **(A)** Change in CT, and MR ECV over time after contrast injection in control subjects (p = 0.208 for CT ECV; p = 0.782 for MR ECV), **(B)** 6-week modeling subjects (p = 0.827 for CT ECV; p = 0.894 for MR ECV), **(C)** 12-week modeling subjects (p = 0.877 for CT ECV; p = 0.691 for MR ECV), and **(D)** 16-week modeling subjects (p = 0.916 for CT ECV; p = 0.831 for MR ECV). ECV = extracellular volume fraction; other abbreviations as in Figure 1.

0.967 (95% CI: 0.899 to 1.000), respectively. There was no significant difference between areas under the receiver operating characteristic curve.

HISTOLOGY. Collagen fibers located in the extracellular space were stained red following picrosirius red staining. The CVF showed a steady increase according to the modeling time (Figure 6).

The mean CVF of the control subjects (n = 4) was 3.3% (2.9% to 4.1%). The mean CVF of 6 (n = 3), 12 (n = 3), and 16 (n = 5) week models was 12.7% (11.4% to 14.1%), 20.1% (16.7% to 25.2%), and 29.3% (19.3% to 38.3%), respectively. Figure 7 demonstrates the histological examples of the control and modeling subjects.

CT ECV obtained using dual-energy CT correlated with histological CVF findings (n = 15; r = 0.925; p < 0.001). Similarly, MR ECV correlated with histological CVF (n = 15; r = 0.961; p < 0.001).

DISCUSSION

This study aimed to validate ECV fraction using dual-energy CT, and to compare the results with contrast-enhanced CMR values and histological findings for evaluation of diffuse myocardial fibrosis in a doxorubicin-induced DCM rabbit model. CT ECV map software that depicted ECV on a color-coded map with a percentage scale was also developed. Changes in ECV can be determined at a glance using CT ECV maps.

Recently, myocardial fibrosis imaging based on T1-mapping and measurement of ECV has been regarded as a promising tool for detecting and quantifying diffuse myocardial fibrosis (5,6). Nacif et al. (8) reported on the usefulness of myocardial ECV measurements using bolus injection contrast-enhanced CT and found that the cardiac CT and MR ECVs were

TABLE 2 CT and MR ECV and Histologic CVF in All Subjects

	Control Subjects (n = 15)	6-Week Model (n = 11)	12-Week Model (n = 8)	16-Week Model (n = 5)
CT ECV, %	28.5 (25.9–31.3)	35.3* (30.2–40.1)	41.9† (35.6–44.1)	42.1‡ (39.2–46.4)
MR ECV, %	28.8 (26.1–30.8)	32.6* (29.9–34.3)	35.8† (31.0–39.8)	41.3‡ (38.4–47.3)
CVF, %	3.3§ (2.9–4.1)	12.7‖ (11.4–14.1)	20.1‖ (16.7–25.2)	29.3¶ (19.3–38.3)
Pre-T1, ms	1,068.1 (1,030.0–1,103.85)	1,110.3* (1,075.2–1,175.0)	1,118.2† (1,059.2–1,160.8)	1,121.3‡ (1,104.5–1,121.8)
Post-contrast HU	58.0 (51–70)	60.2 (50–77)	68.4† (61.2–76.9)	69.4‡ (62.6–73.1)

Values are mean (range). *Control vs. 6-week model, $p < 0.05$. †Control vs. 12-week model, $p < 0.05$. ‡Control vs. 16-week model, $p < 0.05$. §n = 4. ‖n = 3. ¶n = 5.
CMR = cardiac magnetic resonance; CT = computed tomography; CVF = collagen volume fraction; ECV = extracellular volume fraction; HU = Hounsfield unit.

higher in patients with heart failure than in healthy control subjects. Additionally, the results indicated a good correlation between cardiac CT ECV and MR ECV values (8).

In a separate study, Bandula et al. (7) developed and validated an equilibrium contrast-enhanced CT protocol involving continuous infusion after bolus injection. Equilibrium CT ECV was strongly correlated to equilibrium MR ECV, and exhibited a significant correlation with histological fibrosis. Thus, prior studies have demonstrated the possibility of quantifying myocardial fibrosis using cardiac CT. In the current study, we sought to establish the validity of dual-energy CT by CT ECV measurement and compare

FIGURE 4 Examples of CT ECV Maps in Control and Models

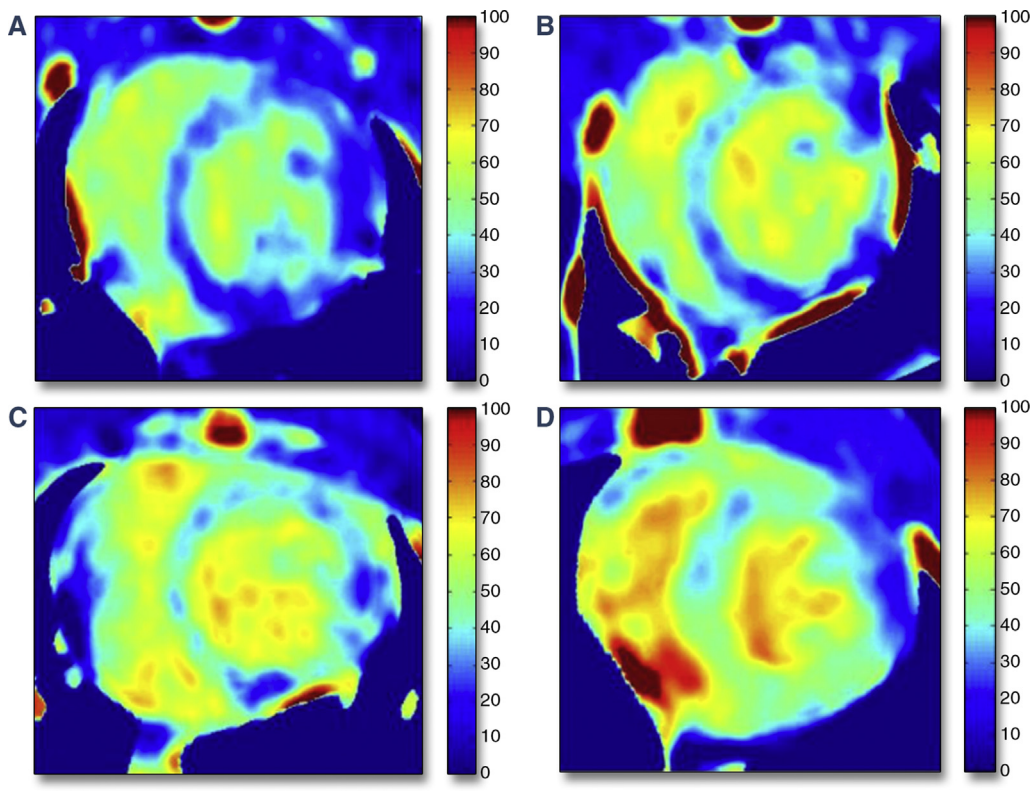

(A) Control subject (Hct = 44.4%), ECV = 27.0%; **dark blue** normal myocardium shown on the ECV map. **(B)** Six-week model (Hct = 37.4%), ECV = 36.4%; **dark blue** septal wall changed to **bright blue**. **(C)** Twelve-week model (Hct = 30.0%), ECV = 44.0%; **dark blue** area of inferoseptal/inferolateral wall changed to **bright blue** myocardium. **(D)** Sixteen-week model (Hct = 25.0%), ECV = 46.0%; **bright blue** myocardium suggests myocardial fibrosis. Hct = hematocrit; other abbreviations as in Figures 1 and 3.

it with MR ECV for evaluating diffuse fibrosis in doxorubicin-induced cardiotoxicity in a rabbit model.

CT offers several advantages over MR, including coverage of the whole myocardium in a short scanning time, and widespread availability (7). Additionally, CT can be substituted for CMR in case of contraindications (e.g., CMR-unsafe devices and claustrophobia).

However, previous studies used conventional CT with both pre-contrast and post-contrast equilibrium CT (7,8). For the analyses, ROIs in the myocardial septum were selected on the post-contrast image, whereas the corresponding areas on the pre-contrast image were selected by visual estimation. This method led to mis-registration errors because of changes in the pre-contrast and post-contrast CT acquisition location. More importantly, the radiation exposure was doubled.

Consequently, the method used in the current study was changed to dual-energy CT, which uses data acquired at the time of the scan to produce both pre-contrast and post-contrast images. Moreover, dual-energy CT can simultaneously provide data from CT images obtained at 2 different x-ray spectra (10). Difference in material composition was shown because the different photon absorption rates were affected by the data in the 2 spectra (10,16). In this study, the major advantages of dual-energy CT were the lack of mis-registration errors that occurred from pre-contrast and post-contrast scanning with different scanning times and at different positions. An iodine map was simultaneously reconstructed from contrast image data acquired at 100 and 140 kVp. The one scan was sufficient to visualize delayed contrast-enhancement, thus eliminating the requirement for the 2-step process of obtaining pre-contrast and post-contrast scans.

This study is the first to assess CT ECV using dual-energy CT. To determine the proper scanning parameters and to find the stabilization point for CT ECV, scans were performed at 3, 5, 7, 9, 11, 13, and 20 min after contrast injection. CMR scans were also performed at those time points for comparison. CT ECV values did not significantly change throughout the scanning in all subjects. The MR ECV in this study was also stabilized at 3 min after contrast injection. The previous studies showed similar result that human ECV stabilized at approximately 5 min after contrast injection (17–19).

Equation 2 was used for calculating ECV values. In the dual-energy CT measurement, the corresponding HU of the ROI on the iodine map represented the degree of enhancement of the measured area. The HU of the ROI on the iodine map was sufficient to measure HU in the myocardium and blood cavity. A software program that measured CT ECV and generated a color-coded iodine map illustrating the distribution of iodine contrast in the myocardium was developed. Furthermore, the software enabled quantification of the myocardial enhancement using the HU reported on the iodine map. Although

FIGURE 5 Bland-Altman Plots for the CT and MR ECV on Per Subject Analysis

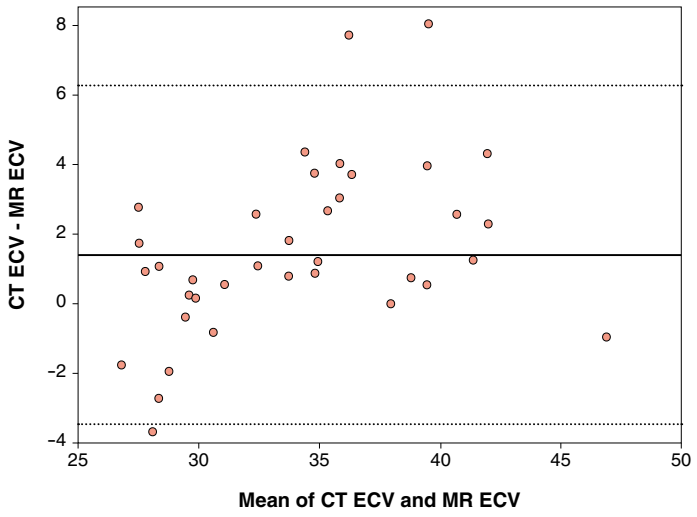

Small bias (1.406%) was noted with 95% limits of agreement from -3.457% to 6.269% between CT and MR ECV. Abbreviations as in Figures 1 and 3.

FIGURE 6 Mean Histological CVF (%) in the Control and Models

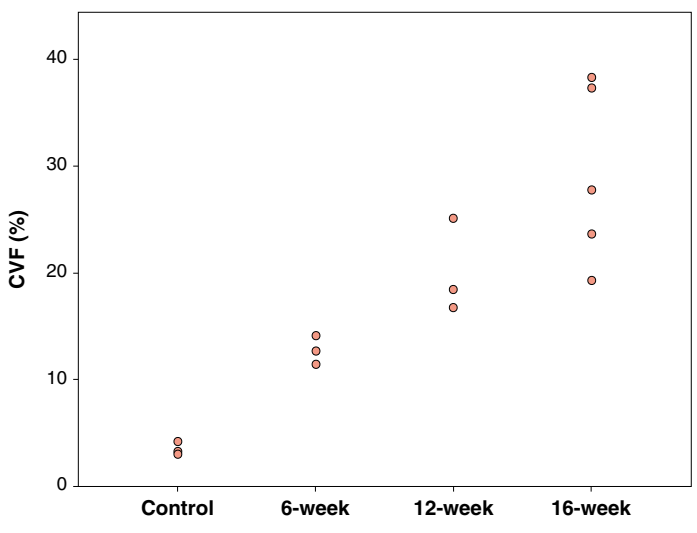

The graph showed a steady increase of CVF according to the modeling time. CVF = collagen volume fraction.

FIGURE 7 The Histological Example of the Control and 6-, 12-, and 16-Week Models

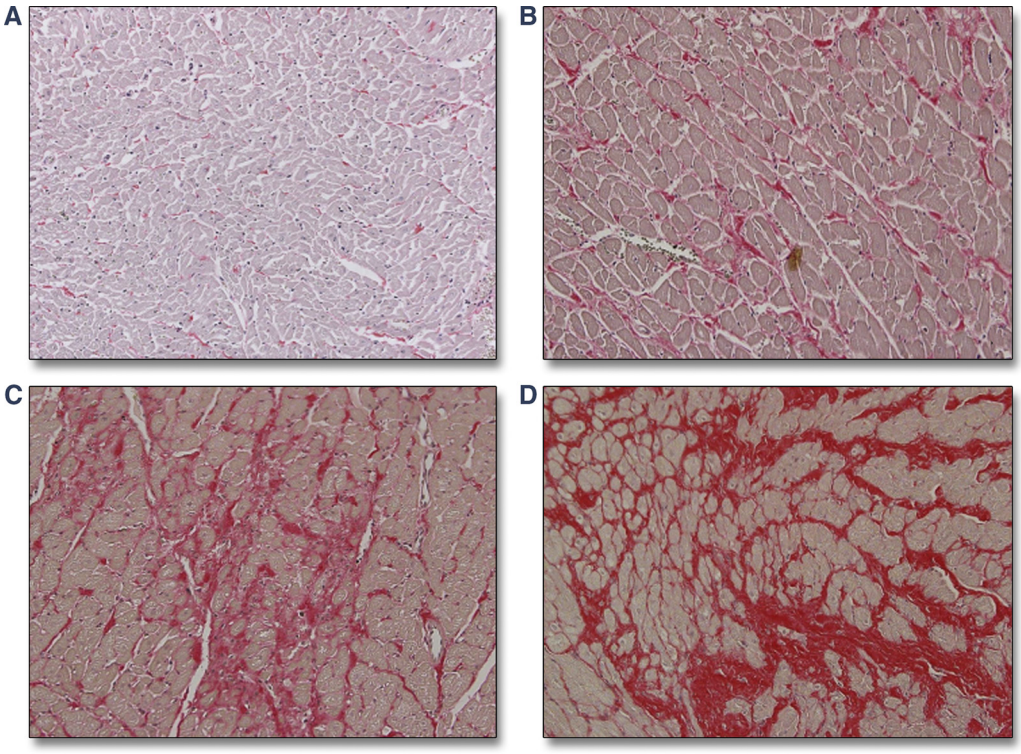

Collagen volume fraction values **(A)** 2.1%, **(B)** 11.8%, **(C)** 24.9%, and **(D)** 44.7%, respectively (picrosirius red, original magnification ×200).

CMR has been the standard for imaging fibrosis, the potential benefits of CT warrant recognition because CT enables rapid, widely available, and economical imaging.

In addition, this study demonstrated proof of concept using an animal model. Further studies are required for assessment in humans. The estimated radiation dose for humans would be 3 to 4 mSv (20). When considering hazards of CT, clinical utility of CT ECV in high-risk cancer patients is quite limited. An additional method (e.g., iterative reconstruction) might lower the radiation burden and make this technique feasible for clinical application in humans.

STUDY LIMITATIONS. The limitations of the current study included the small sample size and motion artifacts from the fast heart rate or arrhythmia of the rabbits. Although a drug was used to reduce heart rate, the mean heart rates of the pre-modeling and post-modeling animals were 114.3 ± 13.0 beats/min and 98.2 ± 8.2 beats/min, respectively. Such a high heart rate would not be encountered in humans. However, arrhythmia would be encountered frequently. Retrospective gating mode would be helpful for acquiring accessible image quality. However, considerable amount of radiation exposure will still be a problem. CT ECV was correlated with histological assessments of CVF. Because there is no direct method for measuring histological ECV, the relationship between CT ECV and histological ECV could not be evaluated. Nonetheless, the correlation between CT ECV and histological CVF was statistically significant. Our study showed that ECV changes can be detected by using both MR and CT, and that these are comparable with the significant changes in LVEF determined using CMR. CMR ejection fraction can be adequate for detection of cardiotoxicity based on the result of the study in which the diagnostic values of CT, MR ECV, and ejection fraction in detecting cardiotoxicity were not significantly different. Further study is required to determine the most sensitive method for early detection of cardiotoxicity.

CONCLUSIONS

This study demonstrated that dual-energy CT for computing CT ECV is a feasible, noninvasive method for quantitatively measuring diffuse myocardial

fibrosis. However, further technical improvements are desirable to lower motion artifact and radiation exposure.

ACKNOWLEDGMENTS The authors thank Professor Yeon Hyeon Choe (Department of Radiology, Samsung Medical Center, Sungkyunkwan University School of Medicine), Professor Hye-Yeon Lee (Department of Anatomy, Yonsei University College of Medicine), and Professor Young-Guk Ko (Department of Cardiology, Yonsei University College of Medicine).

REPRINT REQUESTS AND CORRESPONDENCE: Dr. Byoung Wook Choi, Department of Radiology, Research Institute of Radiological Science, Severance Hospital, Yonsei University College of Medicine, 50 Yonsei-ro, Seodaemun-gu, Seoul 120-752, South Korea. E-mail: bchoi@yuhs.ac.

PERSPECTIVES

COMPETENCY IN MEDICAL KNOWLEDGE: This pilot study established the necessary steps for conducting a broader examination of dual-energy CT, CMR, and the histological assessment of doxorubicin-induced cardiotoxicity. Although CMR has been the standard for imaging fibrosis, the potential benefits of using dual-energy CT warrant recognition.

TRANSLATIONAL OUTLOOK: This study demonstrated proof of concept using an animal model. Further studies are required for assessment in humans. When transferring this method for humans, optimal scan parameters, such as the amount of contrast dose, and delayed imaging time should be investigated.

REFERENCES

1. Blum RH, Carter SK. Adriamycin. A new anticancer drug with significant clinical activity. Ann Intern Med 1974;80:249–59.

2. Elbl L, Hrstkova H, Chaloupka V. The late consequences of anthracycline treatment on left ventricular function after treatment for childhood cancer. Eur J Pediatr 2003;162:690–6.

3. Assomull RG, Prasad SK, Lyne J, et al. Cardiovascular magnetic resonance, fibrosis, and prognosis in dilated cardiomyopathy. J Am Coll Cardiol 2006;48:1977–85.

4. Wu KC, Weiss RG, Thiemann DR, et al. Late gadolinium enhancement by cardiovascular magnetic resonance heralds an adverse prognosis in nonischemic cardiomyopathy. J Am Coll Cardiol 2008;51:2414–21.

5. Neilan TG, Coelho-Filho OR, Shah RV, et al. Myocardial extracellular volume by cardiac magnetic resonance imaging in patients treated with anthracycline-based chemotherapy. Am J Cardiol 2013;111:717–22.

6. Tham EB, Haykowsky MJ, Chow K, et al. Diffuse myocardial fibrosis by T1-mapping in children with subclinical anthracycline cardiotoxicity: relationship to exercise capacity, cumulative dose and remodeling. J Cardiovasc Magn Reson 2013;15:48.

7. Bandula S, White SK, Flett AS, et al. Measurement of myocardial extracellular volume fraction by using equilibrium contrast-enhanced CT: validation against histologic findings. Radiology 2013;269:396–403.

8. Nacif MS, Kawel N, Lee JJ, et al. Interstitial myocardial fibrosis assessed as extracellular volume fraction with low-radiation-dose cardiac CT. Radiology 2012;264:876–83.

9. Gerber BL, Belge B, Legros GJ, et al. Characterization of acute and chronic myocardial infarcts by multidetector computed tomography: comparison with contrast-enhanced magnetic resonance. Circulation 2006;113:823–33.

10. Johnson TR, Krauss B, Sedlmair M, et al. Material differentiation by dual energy CT: initial experience. Eur Radiol 2007;17:1510–7.

11. Gava FN, Zacche E, Ortiz EM, et al. Doxorubicin induced dilated cardiomyopathy in a rabbit model: an update. Res Vet Sci 2013;94:115–21.

12. Kellman P, Wilson JR, Xue H, Ugander M, Arai AE. Extracellular volume fraction mapping in the myocardium, part 1: evaluation of an automated method. J Cardiovasc Magn Reson 2012;14:63.

13. Hamlett A, Ryan L, Serrano-Trespalacios P, Wolfinger R. Mixed models for assessing correlation in the presence of replication. J Air Waste Manag Assoc 2003;53:442–50.

14. Bland JM, Altman DG. Agreement between methods of measurement with multiple observations per individual. J Biopharm Stat 2007;17:571–82.

15. Obuchowski NA. Nonparametric analysis of clustered ROC curve data. Biometrics 1997;53:567–78.

16. Graser A, Johnson TR, Chandarana H, Macari M. Dual energy CT: preliminary observations and potential clinical applications in the abdomen. Eur Radiol 2009;19:13–23.

17. Kawel N, Nacif M, Santini F, et al. Partition coefficients for gadolinium chelates in the normal myocardium: comparison of gadopentetate dimeglumine and gadobenate dimeglumine. J Magn Reson Imaging 2012;36:733–7.

18. Kawel N, Nacif M, Zavodni A, et al. T1 mapping of the myocardium: intra-individual assessment of the effect of field strength, cardiac cycle and variation by myocardial region. J Cardiovasc Magn Reson 2012;14:27.

19. Lee JJ, Liu S, Nacif MS, et al. Myocardial T1 and extracellular volume fraction mapping at 3 tesla. J Cardiovasc Magn Reson 2011;13:75.

20. Wichmann JL, Arbaciauskaite R, Kerl JM, et al. Evaluation of monoenergetic late iodine enhancement dual-energy computed tomography for imaging of chronic myocardial infarction. Eur Radiol 2014;24:1211–8.

KEY WORDS cardiac imaging techniques, cardiomyopathy, dual-energy scanned projection, magnetic resonance imaging, mapping, radiography

APPENDIX For a supplemental figure and materials, please see the online appendix.